Astron. Astrophys. 264, 637–653 (1992)

ASTRONOMY AND ASTROPHYSICS

The β Pictoris circumstellar disk

XIII. Survey of the variable Ca II lines*

A.M. Lagrange-Henri[1], E. Gosset[2], H. Beust[3], R. Ferlet[3], and A. Vidal-Madjar[3]

[1] Groupe d'Astrophysique de Grenoble, Université J. Fourier, BP 53X, F-38041 Grenoble Cédex, France
[2] Institut d'Astrophysique, Université de Liège, 5 Avenue de Cointe, B-4000 Liège, Belgium
[3] Institut d'Astrophysique de Paris, CNRS, 98 bis boulevard Arago, F-75014 Paris, France

Received November 4, 1991; accepted June 2, 1992

Abstract. We present here more than 200 Ca II K and H spectra of β Pictoris taken between Sept. 19, 1989 and Dec. 19, 1990. A lot of new variable features are observed, at small and high redshifts, together with a few blueshifted ones. The time scales for the variations are shown to be strongly dependent on the redshift of the variable lines. From this survey, we derive a rate of events of ≃ 200 per year; we also show that in some cases the absorbing cloud covers less than 40 per cent of the stellar surface. The observed variations are analysed, and compared to those observed in the UV. These observations provide a unique opportunity to test our scenario of evaporating infalling bodies, in terms of velocity of variable lines, occurrence of variable events, small time scale variations and size of the absorbing cloud. We show that the observed velocity range for the variable components may be explained by this scenario, as well as the size of the absorbing clouds. New physical parameters are suggested to improve the present simulation but the main conclusions do not change. It also seems that the present statistics of events is not yet sufficient to definitely test the possible presence of a large perturbing body around β Pictoris, although the main characteristics of the present data are consistent with the predictions of such a model.

Key words: stars: circumstellar matter – stars: β Pictoris – observational methods

1. Introduction

The disk of dust and gas around β Pictoris is now widely regarded as a protoplanetary system, in a still unknown state of evolution (for a review on this topic, see for instance Norman & Paresce 1989). Extensive observations in the UV with IUE (30 km s^{-1} spectral resolution) have shown strong variations in the circumstellar (CS) lines of ionized elements (Fe II, Al III, Mg II). More precisely, we sometimes observe in addition to a central circumstellar absorption (i.e. at the velocity of the stellar line, within 2 km s^{-1}), redshifted components with redshifts depending on the ions, and sometimes as high as 300 km s^{-1}. These variable lines have been attributed to the evaporation of cometary like bodies falling on to the star (Lagrange-Henri et al. 1987 (Paper IV); Ferlet et al. 1987 (Paper V); Lagrange-Henri et al. 1988 (Paper VI)). An estimation of the size of the bodies necessary to reproduce the observed amount of variable gas in the UV led to typical sizes of 1 kilometer. Variable lines were also observed in January 1986 at higher resolution (3 km s^{-1}), in the Ca II K line (Paper V), but at a redshift of about 20 km s^{-1} with respect to the star, i.e. much smaller than those observed in the UV lines. Comparing the two resonance lines of the Al III doublet, we also showed that these two lines were saturated without reaching the zero level intensity. No instrumental effect could explain the observed features, and the conclusion was then that the Al III cloud responsible for the redshifted absorption lines was clumpy (Lagrange-Henri et al. 1989 (Paper VIII)). This again was in favor of our model of evaporating bodies.

The "evaporating infalling bodies" (hereafter EIB) scenario has been quantitatively tested by Beust et al. (1989 (Paper IX); 1990 (Paper X)), who simulated the evaporation of cometary like bodies grazing the star, on parabolic orbits with close perihelions (a few stellar radii). The grains evaporated from the comet were assumed to produce the evaporated ions; these ions were supposed to be submitted to gravity, radiation pressure and collisions with surrounding gas and grains. Their motion was then followed and the resulting absorption lines computed. This simulation enabled us to satisfactorily reproduce the velocity and shape of the Ca II variable line observed in January 1986 as well as the highly redshifted UV lines, once given appropriate values for the orbital parameters of the comet (in fact, the perihelion of the orbit and the inclination of the axis of the orbit with respect to the line of sight). Roughly, the Ca II variable component at 20 km s^{-1} could be reproduced with an inclination of $\Phi = -150°$ and a perihelion q of about $20R_*$, while the highly redshifted UV lines were reproduced with a similar inclination, but with a much smaller perihelion (about $3R_*$). Moreover, the radiation pressure was shown to strongly differ from one ion to the other; this could explain quite well the differences observed in the variable lines of the different ions (paper IX).

In a recent paper, Beust et al. (1991b) (Paper XII) simulated the infall of cometary like bodies perturbed by a planet orbiting around β Pictoris, to investigate the dependence of the rate of infall as a function of time. Using the observations available at

Send offprint requests to: A.M. Lagrange

*Based on observations collected at the European Southern Observatory, La Silla, Chile.

that time, they tentatively suggested that those observations could be explained by the presence of a large planet on a very eccentric orbit. They also predicted the future behaviour of the spectral variations in both frequency and redshifts of events. However, they also pointed out the need of new data to definitely assess this scenario.

Recently, the EIB scenario has been questioned by Grady et al. (1991), on the basis of the comparison of β Pictoris spectra with those of some Be shell stars : in one case, infalling gas was detected in UV lines whereas there is no evidence for dust around this particular star (no IR excess). This led them to consider other mechanisms to explain the infalling gas. In particular, they suggested that gas might have been expelled by the star without reaching the escape velocity. According to them, a similar scenario could be responsible for the infalling events detected towards β Pictoris. However, the infall velocity observed for that star is much smaller (typically 20 km s^{-1}) than what we observe for β Pictoris. Moreover, contrary to those Be shell stars which indeed sometimes show strong blueshifted features, possibly due to expelled gas, β Pictoris, which is an A5 star, never showed strong evidence for gas expansion.

In a subsequent paper, Bruhweiler et al. (1991) showed a faint blueshifted absorption in an Fe II UV line of β Pictoris. As they noted, the rate of infall seen in the UV is much higher than the rate of outfall. Finally, the authors came to a conclusion similar to ours of Paper VI, i.e. that a "stellar wind" phenomenon cannot alone explain the observations.

In order to further test the EIB scenario, we have to get more information on:

1. the occurrence of variable events;
2. the velocities, duration and small time scale variations of the variable components, in order to determine the orbital parameters necessary to reproduce the observations, so as to complete the theoretical study undertaken in paper XII;
3. the geometry and physical conditions in the absorbing cloud.

High resolution Ca II observations were thus performed at ESO between Sept. 1989 and Dec. 1990. The more than 200 spectra recorded in both H and K lines during this survey are presented and analysed in Sect. 2 and 3, respectively. Two of the most unusual variable components observed at the beginning of this survey, namely a highly redshifted one (80 km s^{-1}) and a centered one, have already been shown in Beust et al. (1991a) (Paper XI), and well reproduced by our simulation, with a different inclination of the orbit of the body compared to the first simulation, leading to a further confirmation of the model. Finally, we discuss in Sect. 4 the whole set of newly gathered data in the frame of our EIB scenario.

2. Observations and analysis procedures

2.1. Observations

2.1.1. Observing log

High resolution Ca II spectra of β Pictoris were recorded between Sept. 1989 and Dec. 1990, with the European Southern Observatory (ESO) Coudé Echelle Spectrometer (CES) fed by the 1.4 m Coudé Auxiliary Telescope (CAT). Most of the observations were made under Remote Control from Garching, the remaining kindly made by different observers at CAT during Dec. 1989/Jan. 1990. The spectral resolving power was either 10^5 (Long Camera Mode) or 60000 (Short Camera Mode), and

Table 1. Log of the observations

Date	U.T.	Exp.(s)	Line	Cam.+Det.	Res.
1989/09/25	07:57	800	K	LC+CCD	100000
1989/09/25	08:57	800	K	LC+CCD	100000
1989/10/20	05:04	2400	K	LC+CCD	100000
1989/10/20	06:01	2100	K	LC+CCD	100000
1989/10/20	07:44	1800	K	LC+CCD	100000
1989/10/20	08:34	600	H	LC+CCD	100000
1989/10/20	08:55	1000	H	LC+CCD	100000
1989/10/20	09:10	500	H	LC+CCD	100000
1989/10/27	04:35	1200	K	LC+CCD	100000
1989/10/27	06:02	1200	H	LC+CCD	100000
1989/10/28	06:01	1800	K	SC+CCD	60000
1989/10/28	06:36	1800	K	SC+CCD	60000
1989/10/28	07:36	1800	H	SC+CCD	60000
1989/10/28	08:05	1000	H	SC+CCD	60000
1989/10/29	08:09	1200	K	SC+CCD	60000
1989/10/29	09:12	1200	K	SC+CCD	60000
1989/11/27	04:52	300	K	SC+CCD	60000
1989/11/27	05:00	300	K	SC+CCD	60000
1989/11/27	05:06	300	K	SC+CCD	60000
1989/11/27	05:12	300	K	SC+CCD	60000
1989/11/27	05:19	300	K	SC+CCD	60000
1989/11/27	06:26	300	K	SC+CCD	60000
1989/11/27	06:33	300	K	SC+CCD	60000
1989/11/28	02:48	900	H	LC+CCD	100000
1989/11/28	03:18	1500	H	LC+CCD	100000
1989/11/28	03:44	1200	H	LC+CCD	100000
1989/11/28	04:17	900	K	LC+CCD	100000
1989/11/28	04:36	1000	K	LC+CCD	100000
1989/11/28	04:56	900	K	LC+CCD	100000
1989/11/28	05:30	900	K	LC+CCD	100000
1989/11/28	05:48	900	K	LC+CCD	100000
1989/11/28	06:03	900	K	LC+CCD	100000
1989/11/28	06:47	1200	K	LC+CCD	100000
1989/11/28	07:09	1200	K	LC+CCD	100000
1989/11/28	07:33	1600	K	LC+CCD	100000
1989/11/28	07:55	900	K	LC+CCD	100000
1989/11/28	08:23	1500	K	LC+CCD	100000
1989/11/28	08:45	1200	K	LC+CCD	100000
1989/11/29	02:14	1800	K	LC+RET	100000
1989/11/29	03:04	2700	K	LC+RET	100000
1989/11/29	04:02	2700	K	LC+RET	100000
1989/11/29	05:02	2700	K	LC+RET	100000
1989/11/29	06:04	2700	H	LC+RET	100000
1989/11/29	07:59	2700	K	LC+RET	100000
1989/11/29	08:43	1200	K	LC+RET	100000
1989/11/30	02:47	3600	K	LC+RET	100000
1989/11/30	04:15	4200	K	LC+RET	100000
1989/11/30	05:44	4200	H	LC+RET	100000
1989/11/30	07:19	4500	K	LC+RET	100000
1989/11/30	08:37	2800	H	LC+RET	100000
1989/12/01	03:10	3600	K	LC+RET	100000
1989/12/01	04:36	4200	H	LC+RET	100000
1989/12/01	06:09	4500	K	LC+RET	100000
1989/12/05	06:32	700	K	SC+CCD	60000
1989/12/06	02:24	600	K	SC+CCD	60000
1989/12/06	06:51	600	K	SC+CCD	60000
1989/12/06	08:33	600	K	SC+CCD	60000
1989/12/07	06:25	600	K	SC+CCD	60000
1989/12/08	02:26	600	K	SC+CCD	60000
1989/12/08	06:27	600	H	SC+CCD	60000
1989/12/17	04:54	480	K	SC+CCD	60000
1989/12/17	05:07	600	K	SC+CCD	60000
1989/12/17	05:22	900	K	SC+CCD	60000

Table 1. (continued)

Date	U.T.	Exp.(s)	Line	Cam.+Det.	Res.
1989/12/18	01:08	900	K	SC+CCD	60000
1989/12/18	01:24	900	K	SC+CCD	60000
1989/12/18	02:58	900	K	SC+CCD	60000
1989/12/18	03:11	600	H	SC+CCD	60000
1989/12/18	03:23	480	H	SC+CCD	60000
1989/12/18	03:33	300	H	SC+CCD	60000
1989/12/20	08:46	1200	K	SC+CCD	60000
1989/12/20	09:10	1000	K	SC+CCD	60000
1989/12/21	05:30	600	K	SC+CCD	60000
1989/12/23	01:01	600	K	SC+CCD	60000
1989/12/25	00:51	600	K	SC+CCD	60000
1989/12/27	01:02	600	K	SC+CCD	60000
1990/01/25	01:26	600	K	SC+CCD	60000
1990/01/25	01:33	600	K	SC+CCD	60000
1990/08/25	08:35	300	K	SC+CCD	60000
1990/08/25	08:48	900	K	SC+CCD	60000
1990/08/26	08:43	900	H	SC+CCD	60000
1990/08/26	09:00	900	H	SC+CCD	60000
1990/08/26	09:18	900	K	SC+CCD	60000
1990/08/26	09:35	900	K	SC+CCD	60000
1990/08/27	08:36	900	K	SC+CCD	60000
1990/08/27	08:52	900	K	SC+CCD	60000
1990/08/28	08:08	300	K	SC+CCD	60000
1990/08/28	08:14	300	K	SC+CCD	60000
1990/08/28	08:20	300	K	SC+CCD	60000
1990/08/28	10:02	300	H	SC+CCD	60000
1990/08/28	10:08	300	H	SC+CCD	60000
1990/09/11	07:27	1800	H	LC+CCD	100000
1990/09/11	07:58	1800	H	LC+CCD	100000
1990/09/11	08:42	1800	K	LC+CCD	100000
1990/09/11	09:13	1800	K	LC+CCD	100000
1990/09/12	07:15	1800	K	LC+CCD	100000
1990/09/12	07:52	2700	K	LC+CCD	100000
1990/09/12	08:40	1800	H	LC+CCD	100000
1990/09/12	09:15	2100	H	LC+CCD	100000
1990/09/14	07:33	1800	K	LC+CCD	100000
1990/09/14	08:05	1800	K	LC+CCD	100000
1990/09/14	08:58	1500	H	LC+CCD	100000
1990/09/14	09:27	1800	H	LC+CCD	100000
1990/09/14	09:58	1800	H	LC+CCD	100000
1990/12/09	01:45	1800	K	LC+CCD	100000
1990/12/09	02:16	1800	K	LC+CCD	100000
1990/12/09	02:47	1800	K	LC+CCD	100000
1990/12/09	03:19	1800	K	LC+CCD	100000
1990/12/09	03:50	1800	K	LC+CCD	100000
1990/12/09	05:01	1800	H	LC+CCD	100000
1990/12/09	05:33	1800	H	LC+CCD	100000
1990/12/09	06:13	1800	H	LC+CCD	100000
1990/12/09	06:34	1800	H	LC+CCD	100000
1990/12/09	06:55	900	H	LC+CCD	100000
1990/12/09	07:12	900	H	LC+CCD	100000
1990/12/09	08:05	1800	K	LC+CCD	100000
1990/12/09	08:29	900	K	LC+CCD	100000
1990/12/09	08:45	900	K	LC+CCD	100000
1990/12/10	02:48	2700	K	LC+CCD	100000
1990/12/10	03:36	2800	K	LC+CCD	100000
1990/12/10	04:46	1800	H	LC+CCD	100000
1990/12/10	05:18	1800	H	LC+CCD	100000
1990/12/10	05:50	1800	H	LC+CCD	100000
1990/12/10	06:59	1800	K	LC+CCD	100000
1990/12/10	07:31	1800	K	LC+CCD	100000
1990/12/10	08:02	1800	K	LC+CCD	100000
1990/12/10	08:33	1800	K	LC+CCD	100000

Table 1. (continued)

Date	U.T.	Exp.(s)	Line	Cam.+Det.	Res.
1990/12/11	01:32	1000	K	LC+CCD	100000
1990/12/11	03:19	600	K	LC+CCD	100000
1990/12/11	06:32	1800	K	LC+CCD	100000
1990/12/11	07:03	1800	K	LC+CCD	100000
1990/12/11	07:34	1800	K	LC+CCD	100000
1990/12/11	08:26	600	H	LC+CCD	100000
1990/12/11	08:47	00	H	LC+CCD	100000
1990/12/12	02:16	2700	K	LC+CCD	100000
1990/12/12	02:56	1900	K	LC+CCD	100000
1990/12/12	03:35	2700	K	LC+CCD	100000
1990/12/12	04:42	1800	H	LC+CCD	100000
1990/12/12	05:13	1800	H	LC+CCD	100000
1990/12/12	05:45	1800	H	LC+CCD	100000
1990/12/12	06:15	1800	H	LC+CCD	100000
1990/12/12	07:07	1800	H	LC+CCD	100000
1990/12/12	07:38	1800	H	LC+CCD	100000
1990/12/13	01:28	2700	K	LC+CCD	100000
1990/12/13	02:30	2700	K	LC+CCD	100000
1990/12/13	03:10	2700	K	LC+CCD	100000
1990/12/13	03:56	2700	K	LC+CCD	100000
1990/12/13	04:41	1800	H	LC+CCD	100000
1990/12/13	05:20	2700	H	LC+CCD	100000
1990/12/13	06:25	1800	K	LC+CCD	100000
1990/12/13	06:56	1800	K	LC+CCD	100000
1990/12/14	01:37	2700	K	LC+CCD	100000
1990/12/14	02:23	2700	K	LC+CCD	100000
1990/12/14	03:30	1800	H	LC+CCD	100000
1990/12/14	04:01	1800	H	LC+CCD	100000
1990/12/14	04:32	1800	H	LC+CCD	100000
1990/12/14	05:06	1800	K	LC+CCD	100000
1990/12/14	05:37	1800	K	LC+CCD	100000
1990/12/14	08:03	1800	K	LC+CCD	100000
1990/12/14	08:34	1800	K	LC+CCD	100000
1990/12/15	01:42	2700	K	LC+CCD	100000
1990/12/15	02:28	2700	K	LC+CCD	100000
1990/12/15	03:54	1800	H	LC+CCD	100000
1990/12/15	04:25	1800	H	LC+CCD	100000
1990/12/15	05:00	1800	H	LC+CCD	100000
1990/12/15	05:56	1800	K	LC+CCD	100000
1990/12/15	06:27	1800	K	LC+CCD	100000
1990/12/15	06:58	1800	K	LC+CCD	100000
1990/12/16	01:46	2700	K	LC+CCD	100000
1990/12/16	02:32	2700	K	LC+CCD	100000
1990/12/16	03:21	2700	K	LC+CCD	100000
1990/12/16	04:07	2700	K	LC+CCD	100000
1990/12/16	04:54	2700	K	LC+CCD	100000
1990/12/16	06:08	1800	H	LC+CCD	100000
1990/12/16	06:47	1800	H	LC+CCD	100000
1990/12/16	07:21	2700	K	LC+CCD	100000
1990/12/16	08:00	1800	K	LC+CCD	100000
1990/12/17	01:25	2700	K	LC+CCD	100000
1990/12/17	02:11	2700	K	LC+CCD	100000
1990/12/17	02:57	2700	K	LC+CCD	100000
1990/12/17	03:43	2700	K	LC+CCD	100000
1990/12/17	04:52	1800	H	LC+CCD	100000
1990/12/17	05:23	1800	H	LC+CCD	100000
1990/12/17	05:57	1800	K	LC+CCD	100000
1990/12/17	06:28	1800	K	LC+CCD	100000
1990/12/17	08:37	1800	K	LC+CCD	100000

the detector either an RCA CCD (ESO CCD #9) or a 1872 photodiode Reticon, both with a pixel size of 15 μm.

In table 1 are given the dates of observations and observing conditions (instrumentation, exposure times, etc) for each night. Whenever possible, we recorded both H and K spectra each night. The number of spectra per night varies between one and

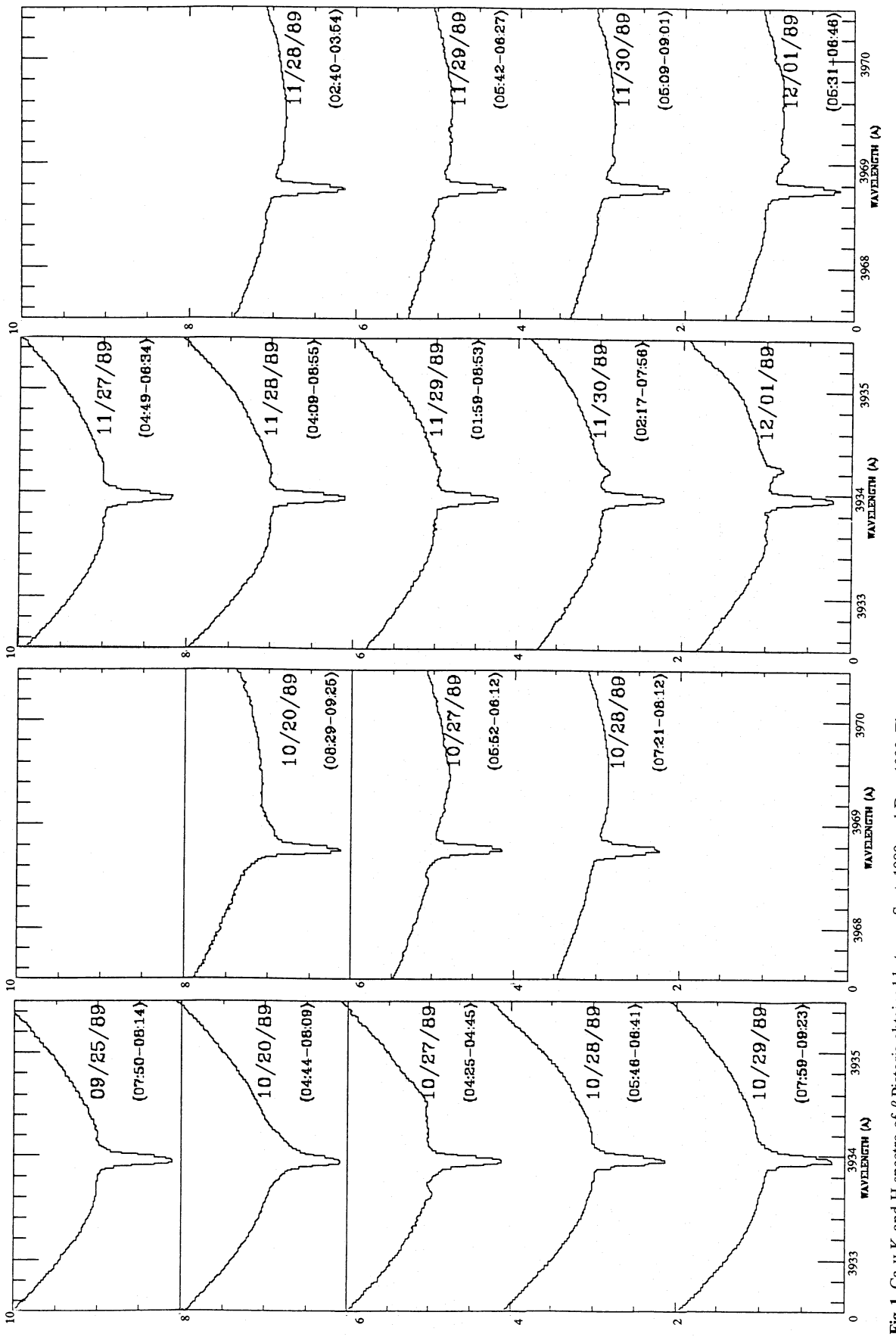

Fig. 1. Ca II K and H spectra of β Pictoris obtained between Sept. 1989 and Dec. 1990. The spectra are averaged over one night. In parentheses are given the start and end Universal Times of the observations. In ordinates, arbitrary units

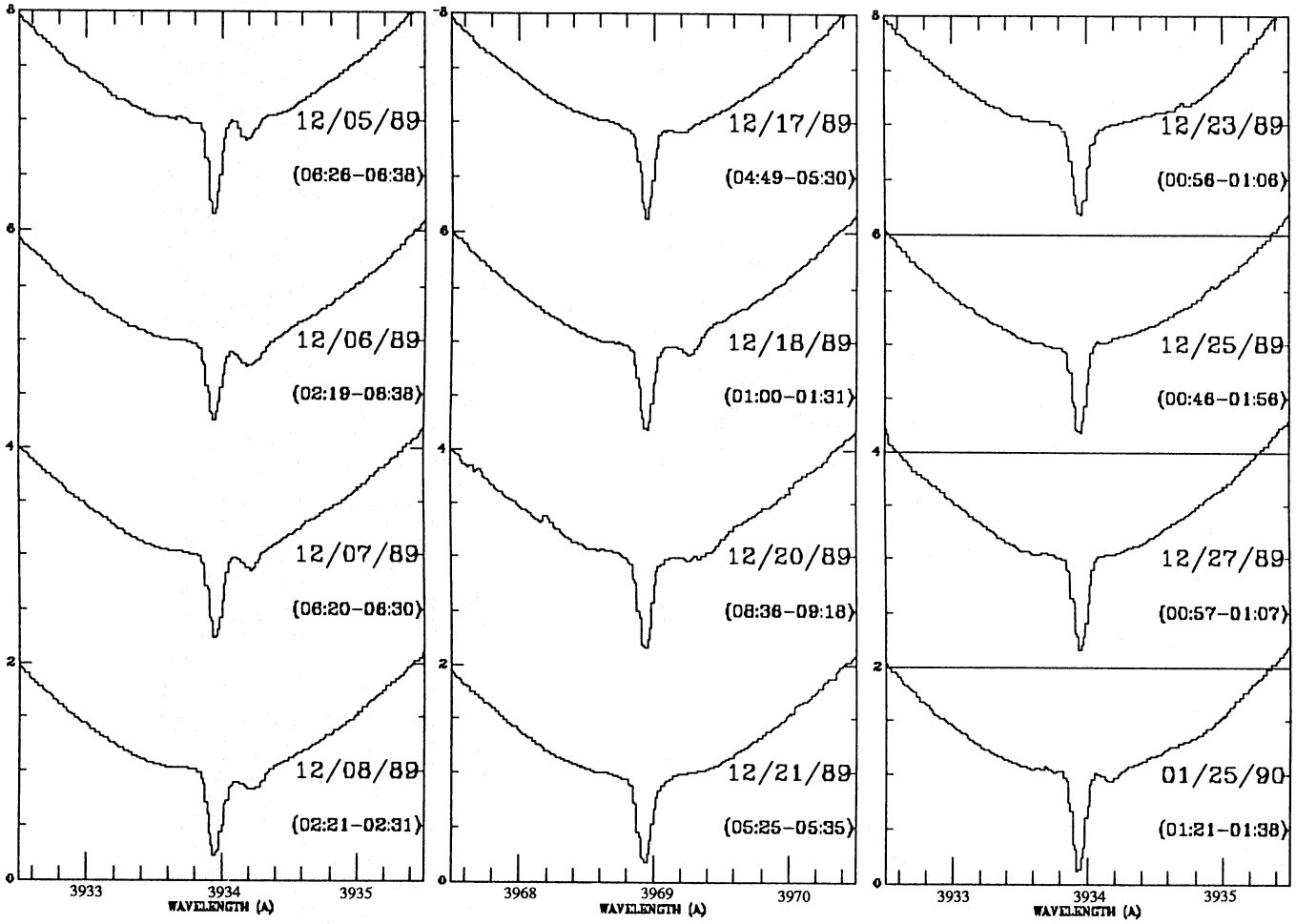

Fig. 1. (continued). The spectra are averaged over one night. In parentheses are given the start and end Universal Times of the observations. In ordinates, arbitrary units

14, depending on observing conditions, and time dedicated to the observation of β Pictoris. In particular, the temporal coverage over each night is quite variable, between 1 hour and the whole night (7 hours). The best temporal coverages were achieved during the periods Nov. 28/Dec. 1, 1989 and Dec. 9/Dec. 17, 1990, where the whole night could be dedicated to the survey. In the first period (Dec. 19, 1989), we had a change of detector, whereas in the second one (Dec. 19, 1990), we kept the same instrumental conditions and the same observing procedure for all the nights, so as to get a very homogeneous set of data.

The exposure time of the observations ranges between five minutes and to more than one hour, depending on the dispersion, on the detector used, and also on weather conditions. Nevertheless, the S/N is always larger than 100 at the bottom of the stellar lines.

2.1.2. Reduction procedure

The CCD data were as usual bias corrected and flatfielded; 1-dimensional (1-D) spectra were then extracted. The Reticon data were dark and bias subtracted and flatfielded. All 1-D spectra were then calibrated by means of thorium-argon spectra. The internal accuracy of the calibration is about 0.5 km s^{-1} for the highest dispersion, and 1 km s^{-1} for the lower one. Usually, thorium spectra were recorded close to the science exposures (less than three hours), in order to account for possible drifts due to temperature variations. We estimate the final accuracy of the calibration to about 1 km s^{-1} (resp. 2 km s^{-1}) for the long (resp. short) camera mode. This standard reduction was made with the ESO IHAP software.

2.1.3. The spectra

Figure 1 shows the Ca II spectra observed during this survey. We show here the spectra averaged over one night. To have an idea of the temporal coverage of the observations, we give the start and end observing times. When significant variations occurred during one night, we give all the spectra obtained during that night (Fig. 2).

2.2. Analysis procedures

2.2.1. Search for variable lines with the IUE-like method

A first aim was to get systematic detection of variable lines. We first tried to use the method developed in the case of the IUE data (see Paper VIII), that is basically to define a reference spectrum, without any variable feature, and to divide all the

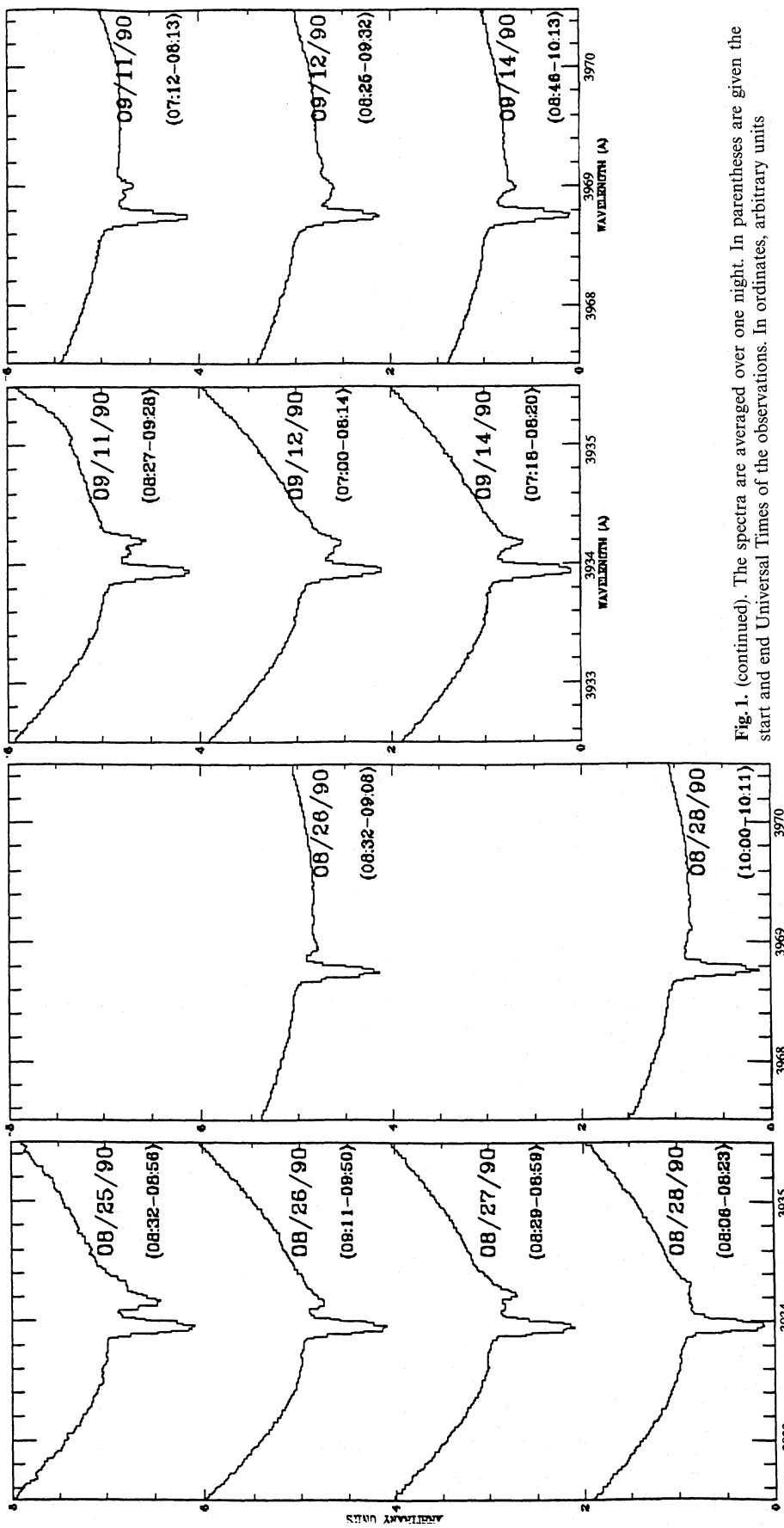

Fig. 1. (continued). The spectra are averaged over one night. In parentheses are given the start and end Universal Times of the observations. In ordinates, arbitrary units

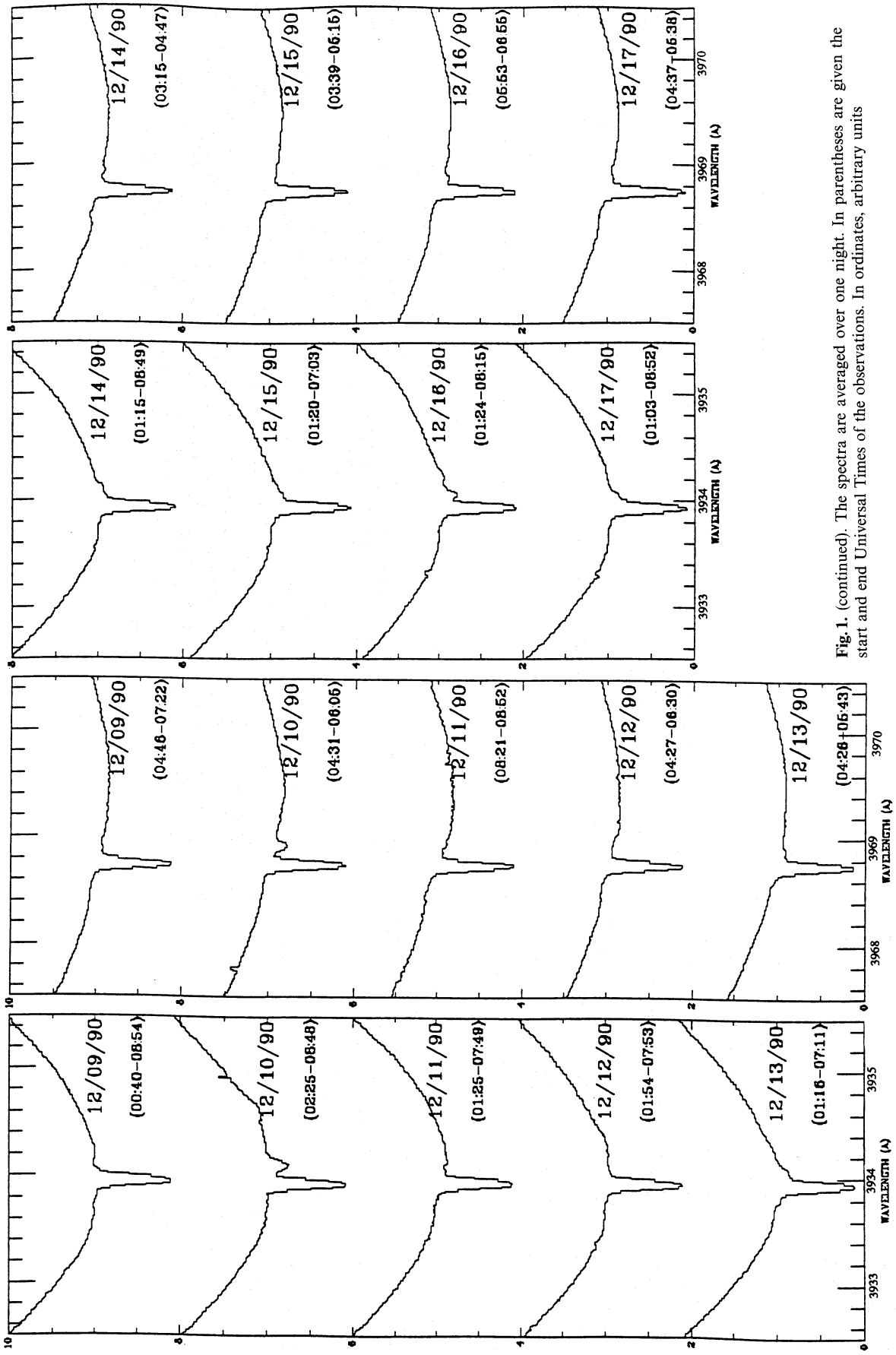

Fig. 1. (continued). The spectra are averaged over one night. In parentheses are given the start and end Universal Times of the observations. In ordinates, arbitrary units

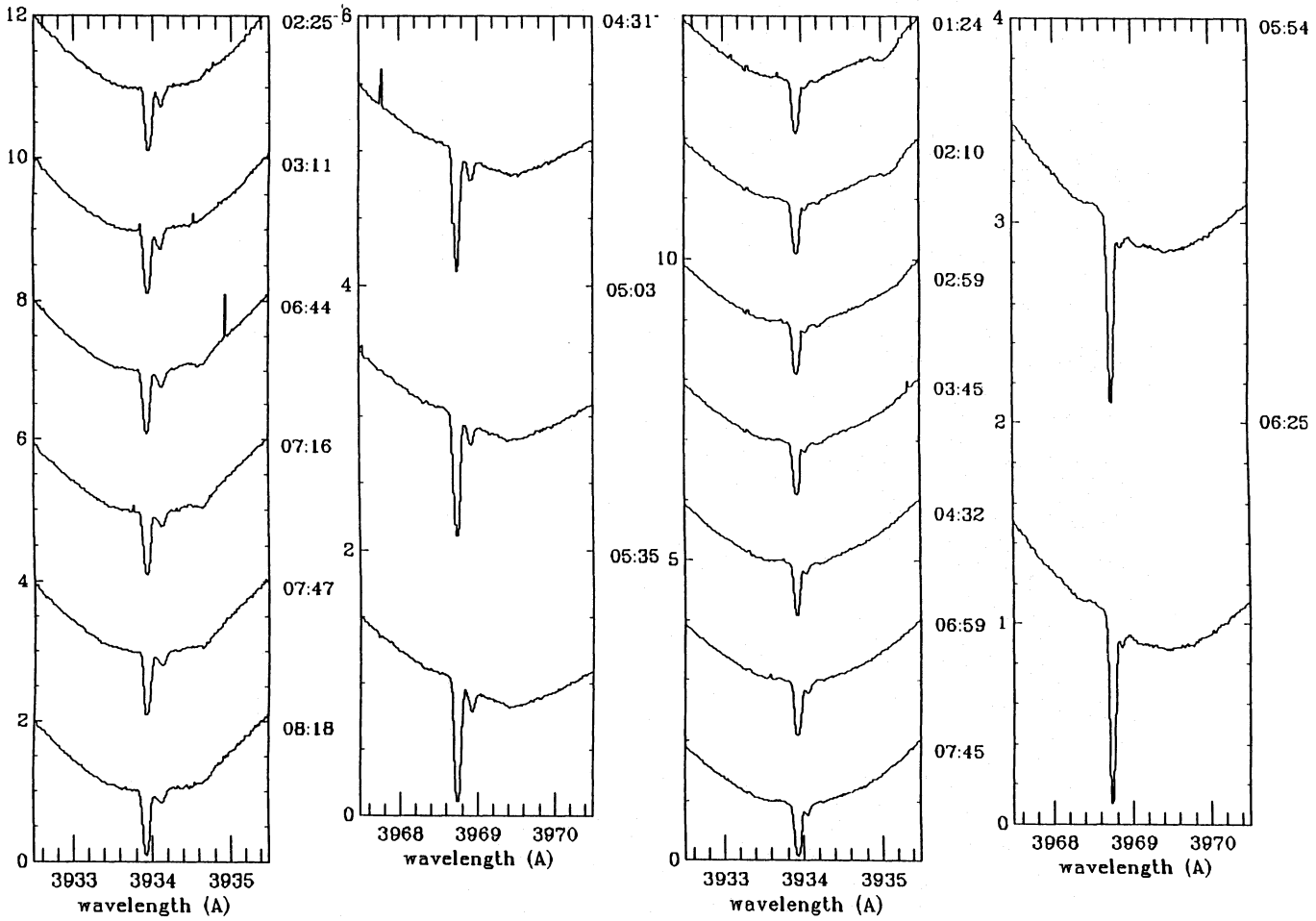

Fig. 2. Small time scale variations in Dec. 1990: (left) Dec. 10, 1990; (right) Dec. 16, 1990. In ordinates, arbitrary units

other spectra by this reference one. In the UV, the result was a remarkably flat spectrum except at wavelengths where variations took place. This method, which worked very satisfactorily for the UV data, does not give good results here. The reason is that the different data are not homogeneous, i.e. have been recorded with different instrumentations and detectors. Differences in the resolution obviously generate artificial features when dividing the spectra; differences in the used detectors also generate problems, because the actual instrumental zero of intensity differs from one detector to the other; this is particularly important in our case where the lines are deep, and thus the error on the true zero larger. In the case of IUE data, all spectra had been recorded with exactly the same observing conditions; moreover, the lines are not as deep; such effects are then not present. Consequently, we use the "IUE" method only for the data recorded in Dec. 1990, when the observing conditions remain very similar for all the nine nights. Figure 3 shows the divided spectra for this period: the divided spectra are quite flat except at wavelengths where variations take place.

Note that even with two spectra taken with the same instrumentation, the division produces artificial P-Cygni-like profiles near the central component which are due to small differences in pixel sensitivities, imperfectly corrected for when the lines are deep. This effect was also observed in the case of IUE data, but to a lower extent, because the lines are not as deep.

2.2.2. Quantitative measurements

In order to get accurate values of the parameters of the variable lines (equivalent widths, FWHM's and velocity positions), we used then the following approach :

For each Ca II K spectrum, the bottom of the photospheric absorption is fitted by a parabola which gives a good fit (see an example in Fig. 4a). Because of the instrumental effects described above, we have to fit each spectrum by a new polynomial. We then divide the spectrum by this "continuum"; the remaining features are assumed to be related to the CS gas. Those features are themselves fitted by gaussians, in order to derive their equivalent widths, FWHM's and velocities. When necessary, we introduce several components for blended absorption features. Figure 4 illustrates the different steps of this procedure which was done using the ESO MIDAS software in Garching. The numerical results are summarized in Table 2. This method enables us to have a good estimate of the parameters (especially the velocity and FWHM) of the different components, particularly in the case of the strongest ones.

Note that after the division by the photospheric fit, some broad and shallow features are often detected (see Table 2), for which it is not straightforward to ascertain they are real or not.

In summary, this method enables us to properly measure only relatively narrow lines and will not be used for the very broad ones.

The Ca II H line has a more complex profile, due to a blend with the strong photospheric H_ϵ line. The parabolic fit is no longer relevant, and we instead used splines. Consequently, the fit is very sensitive to the points used to determine it, and prevents us from detecting features which are not conspicuous. In particular, broad and shallow features will not be detected. Numerical data on Ca II H features are thus available only for sharp lines (see Table 3), except in the case of Dec. 19, 1990 data, where we can divide the spectra.

2.2.3. Search for saturation

In order to get information on the possible saturation of the Ca II lines, and hence on the size of the absorbing clouds, we have to compare the H and K variable features. If α is the ratio of the cloud size to the stellar surface for ions with a given projected radial velocity, we have the following relations :

$$p_H = \alpha \times (1 - e^{-\tau}), \quad \text{and} \tag{1}$$

$$p_K = \alpha \times (1 - e^{-2\tau}) = p_H \times (1 + e^{-\tau}) \quad , \tag{2}$$

where τ is the optical depth of the weakest, H line, and p_H and p_K are respectively the depths of the H and K lines (whose oscillator strengths differ by a factor 2). The ratio p_H/p_K enables us to determine $e^{-\tau}$, and then Eq. 1 provides α. We get:

$$\alpha = \frac{p_H^2}{2p_H - p_K} \quad . \tag{3}$$

Theoretically, this enables us to measure α in any case. However, due to the usually limited quality of the data, such a measurement is not always possible. The uncertainty on α is given by

$$\frac{\Delta\alpha}{\alpha} = \frac{2(p_K - p_H)\,\Delta p_H + p_H\,\Delta p_K}{p_H(2p_H - p_K)}. \tag{4}$$

This is of course valid for $\Delta\alpha/\alpha \leq 1$. Theoretically, we have then to calculate α and $\Delta\alpha$ for each measure (p_H, p_K). However, a preferred approach is the following graphical one: in Fig. 5, we have plotted iso-α curves in a (p_H, p_K) plane. These are parabolae limited by the two lines $p_K = p_H$ and $p_K = 2 \times p_H$. The measured value of (p_H, p_K) enables us then to directly determine α, within the uncertainties given by the error box. One can easily see that for $p_K \simeq p_H$, α will be easily determined, while for unsaturated and weak lines ($p_K \simeq 2 \times p_H$), and especially for small values of p_H, α will not be determined. This physically means that we have no way to distinguish weak lines arising from a cloud covering a small part of the stellar surface, from stronger, but still weak lines, arising from a cloud covering a smaller part of the star. In summary, we will get definite measurements of α only when the lines are almost saturated and not too weak ($p_H \geq 0.05$). When lines are not saturated, we get only a lower limit to the ratio, which would be constraining only for strong variable lines.

Note that all this assumes that the intensities of the lines are very accurately measured; in particular, that the zero intensity level is well defined. Two main effects may in theory affect the zero intensity level: the "resolution effect", and also the possible presence of scattered light into the line of sight, coming from gas anywhere in the surrounding disk. However, as in the case of the Al III lines (see paper VIII), the bottom of the much deeper, nearly satured central component gives an upper limit to these effects (assuming that the stable and the variable lines have comparable widths), and it shows that these effects are certainly negligeable.

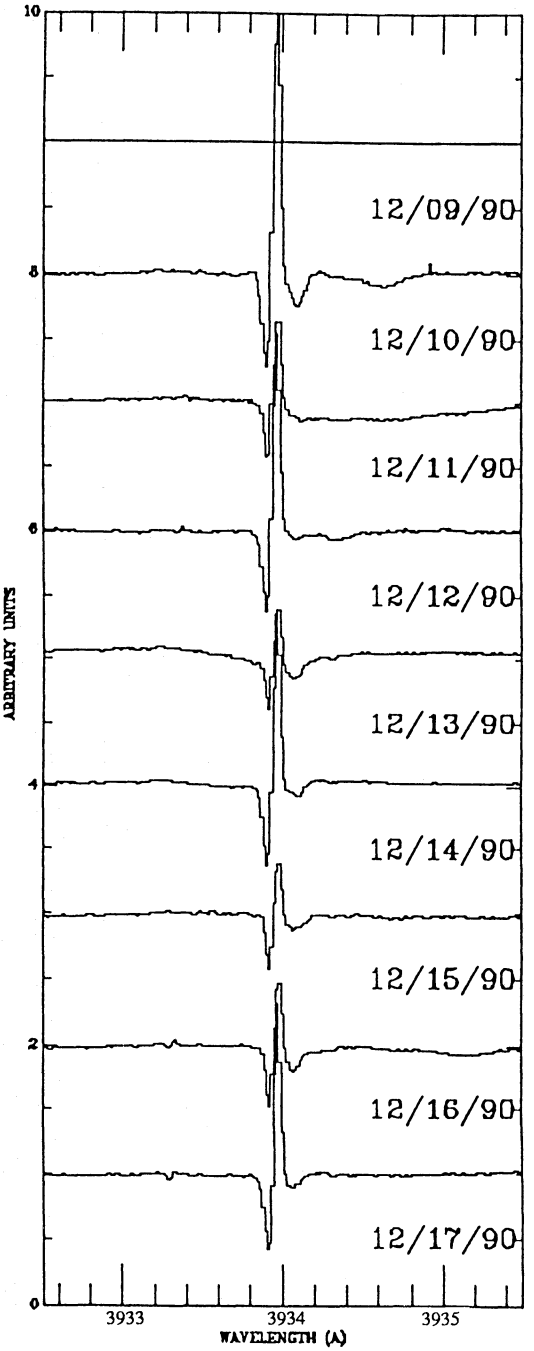

Fig. 3. a) Averaged Ca II K spectra of Dec. 9/17 divided by the average spectra of Dec. 9. In ordinates, arbitrary units

Depending on the observing dates, we will compare either the Ca II K features obtained by the division by the parabolic fit, or those divided by a reference spectrum. In the first case, both the stable and the variable CS lines are present; the uncertainty on p_K and p_H will depend on the quality of the photospheric fit. Noticeably, due to the spline method used for the H line, the uncertainty on p_H may be quite large. A reasonable value for this uncertainty is 0.05. In the second case, the spectra are divided

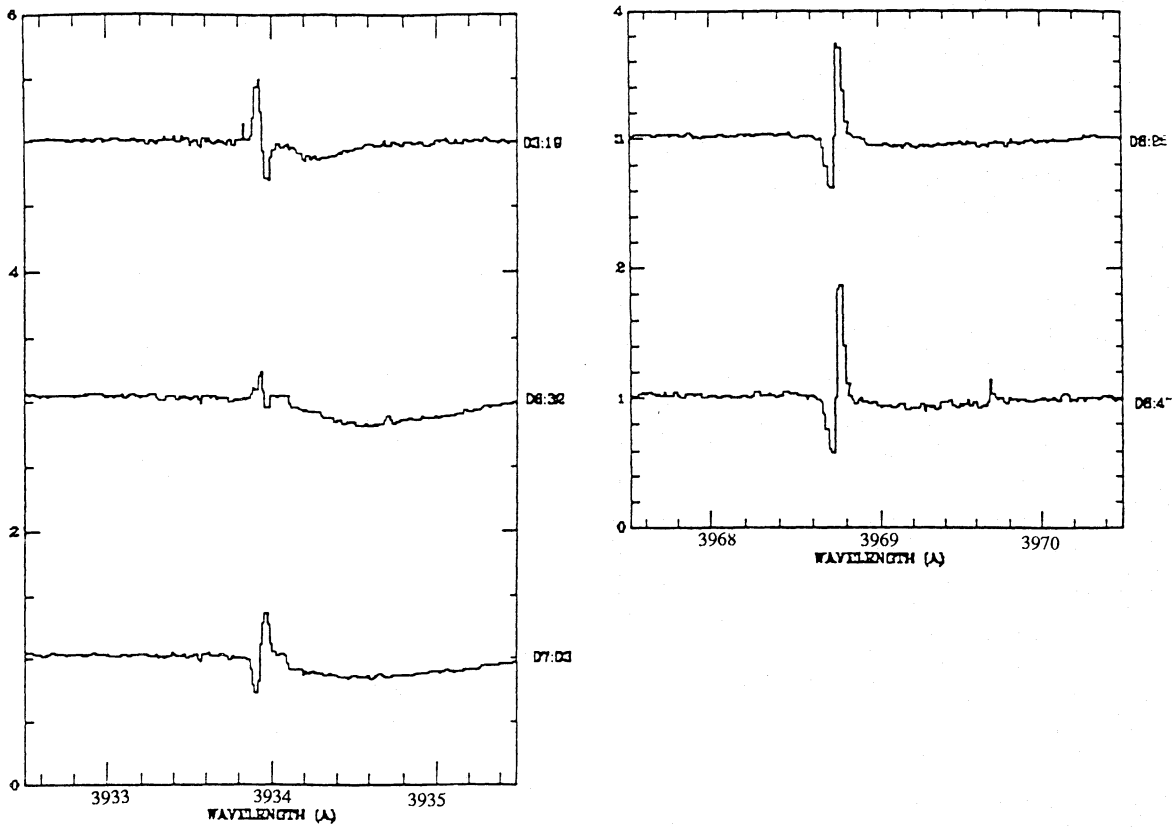

Fig. 3. b) Division of data obtained on Dec. 11 by the one obtained on Dec. 9; left: Ca II K lines; right: Ca II H lines (small time scale variations). In ordinates, arbitrary units

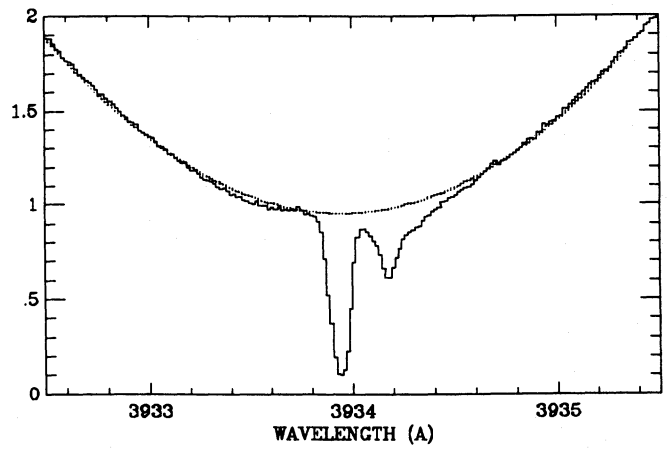

Fig. 4. a) Fit of the photospheric line by a polynomial: the photospheric fit is plotted with dashed lines. In ordinates, arbitrary units

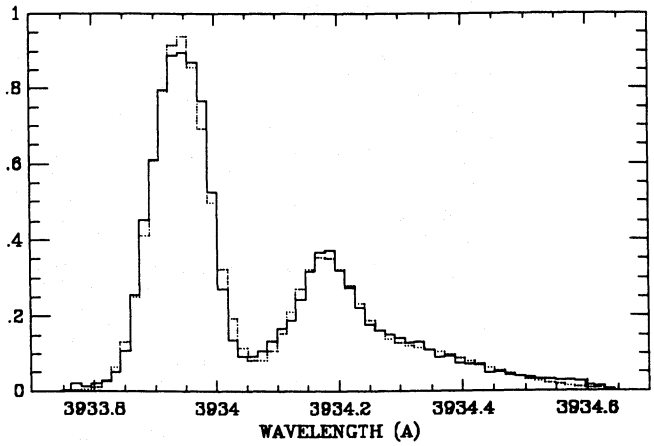

Fig. 4. b) Fit by three gaussians of a variable component obtained after division by the photospheric fit: in bold line, the observed spectrum; in dashed line, the fitted profile. In ordinates, arbitrary units

by a reference spectrum taken with very similar conditions; only variable features are left and the uncertainty may be lower. However, we will somehow conservatively keep the value of 0.05 for Δp_H and Δp_K.

Note that we implicitely assumed that we had to deal with unique, isolated events; if this is not the case, the total depth of the line will be due to blends; however, the previous conclusions remain valid when considering composite clouds with averaged properties and a cumulated filling factor α.

2.2.4. Fourier analysis

In order to further constrain the models, the time variability of different spectral features has been investigated. We used Fourier techniques adapted to unevenly sampled events (Deeming 1975; Scargle 1972). However, the data (FWHM's, equivalent widths) have first to be corrected for systematic differences due to the inhomogeneity of the observations (use of different detectors, at different resolutions). First, to correct for the effect of the various

Table 2. Parameters of the Ca II K variable components, deduced from the analysis described in Sect. 2.2.2.

date	helio. vel. ($km\,s^{-1}$)	eq. width ($\AA$)	fwhm ($\AA$)
1989/09/25	-13.3	0.029	0.509
" "	22.1	0.104	0.107
" "	39.7	0.021	0.404
1989/10/20	21.8	0.067	0.100
" "	25.7	0.139	0.408
1989/10/27	-4.4	0.011	0.151
" "	21.7	0.100	0.102
" "	67.0	0.039	0.368
1989/10/28	-3.7	0.011	0.523
" "	22.3	0.090	0.101
" "	36.9	0.025	0.934
1989/10/29	-0.4	0.076	0.969
" "	22.8	0.089	0.105
1989/11/27	-16.8	0.025	0.50
" "	21.8	0.100	0.112
" "	45.7	0.004	0.140
1989/11/28	-16.4	0.031	0.516
" "	21.2	0.098	0.098
" "	46.9	0.009	0.241
1989/11/29	-18.5	0.012	0.388
" "	21.2	0.084	0.100
" "	43.4	0.014	0.220
1989/11/30	-12.2	0.018	0.448
" "	21.9	0.083	0.097
" "	42.3	0.014	0.110
" "	102.5	0.012	0.422
1989/12/01	-16.6	0.015	0.314
" "	22.0	0.081	0.090
" "	36.7	0.006	0.085
" "	44.1	0.018	0.083
" "	100.8	0.024	0.399
1989/12/05	-17.5	0.027	0.491
" "	21.5	0.095	0.105
" "	40.7	0.029	0.133
" "	59.7	0.013	0.238
1989/12/06	-15.6	0.021	0.467
" "	21.0	0.094	0.122
" "	41.1	0.054	0.202
" "	56.4	0.009	0.186
1989/12/07	5.9	0.106	1.210
" "	22.3	0.084	0.112
" "	42.6	0.028	0.165
1989/12/08	-17.2	0.012	0.372
" "	22.2	0.100	0.121
" "	42.5	0.051	0.240
1989/12/18	21.5	0.089	0.104
" "	42.6	0.008	0.136
12/19/89	2.6	0.080	0.916
" "	21.9	0.093	0.115
" "	45.5	0.028	0.167
1989/12/20	9.2	0.072	1.032
" "	20.8	0.096	0.113
" "	51.5	0.031	0.307
1989/12/21	-8.8	0.020	0.411
" "	21.8	0.103	0.116
" "	44.5	0.012	0.336
1989/12/23	22.0	0.110	0.127
" "	88.3	0.050	0.521

Table 2. (continued)

date	helio. vel. ($km\,s^{-1}$)	eq. width ($\AA$)	fwhm ($\AA$)
1989/12/25	-1.2	0.042	0.584
" "	21.8	0.096	0.111
" "	37.5	0.002	0.068
1989/12/27	-8.8	0.020	0.411
" "	21.8	0.103	0.116
" "	44.5	0.012	0.336
1990/01/25	-20.7	0.019	0.548
" "	21.0	0.101	0.107
" "	39.3	0.015	0.142
" "	91.4	0.006	0.221
1990/08/25	22.0	0.108	0.109
" "	37.5	0.050	0.101
" "	47.0	0.057	0.206
1990/08/26	-13.8	0.015	0.390
" "	22.1	0.107	0.107
" "	37.6	0.021	0.106
" "	46.7	0.031	0.297
1990/08/27	-7.2	0.022	0.421
" "	22.3	0.110	0.110
" "	33.4	0.008	0.065
" "	43.5	0.054	0.180
1990/08/28	-5.0	0.049	0.688
" "	22.5	0.091	0.101
" "	34.5	0.055	0.425
" "	48.8	0.008	0.100
1990/09/11	21.0	0.110	0.111
" "	33.6	0.025	0.083
" "	41.4	0.038	0.084
1990/09/12	21.4	0.110	0.111
" "	37.9	0.090	0.196
" "	54.7	0.030	0.297
1990/09/14	21.3	0.108	0.108
" "	39.1	0.032	0.112
" "	47.5	0.042	0.321
1990/12/09	-11.8	0.022	0.438
" "	20.7	0.095	0.094
" "	30.7	0.006	0.069
1990/12/10	20.4	0.092	0.087
" "	33.7	0.028	0.110
" "	70.5	0.035	0.380
1990/12/11	-15.0	0.018	0.407
" "	21.4	0.086	0.090
" "	43.2	0.033	0.398
" "	77.0	0.149	1.146
1990/12/12	20.9	0.094	0.093
" "	47.4	0.023	0.334
1990/12/13	20.8	0.100	0.100
" "	32.3	0.027	0.152
1990/12/14	21.0	0.096	0.094
" "	33.1	0.013	0.126
1990/12/15	20.9	0.090	0.090
" "	31.3	0.024	0.248
1990/12/16	21.0	0.096	0.093
" "	30.7	0.013	0.066
" "	112.2	0.020	0.385
1990/12/17	20.4	0.096	0.095
" "	30.0	0.007	0.071

resolutions used, we degraded the data to the lowest resolution, i.e. 60000. The correction for the differences in equivalent widths measured with the CCD and the Reticon will be explained later.

3. Results

3.1. Velocities of variable features; small time scale variations; saturation

A first result of this survey is that, in addition to the central component (i.e. at the stellar radial velocity), variable lines are very often clearly present. These variable features are of different types:

- strong (100 mÅ equivalent width) and quasi-centered ($v \simeq 4\ km\,s^{-1}$ (the velocities are given here and hereafter with respect to the star)) absorptions: this kind of feature is observed once (Oct. 20, 1989) both in Ca II K and Ca II H lines. It spreads between -40 and $+40\ km\,s^{-1}$ with respect to the star. These features do not show evidence of variability over the observing period (4 hours).

In Fig. 6, we show the superposition of the K and H CS features obtained after division by the photospheric fit. The red part of the feature is obviously more saturated than the blue part. Quantitatively, if we measure (p_H, p_K) at different velocities, and put them on the (p_H, p_K) diagram (Fig. 5), we

Table 3. Same as Table 2, but for the Ca II H components

date	helio. vel. ($km\,s^{-1}$)	eq. width ($\AA$)	fwhm ($\AA$)
1989/10/20	21.9	0.066	0.084
" "	27.6	0.095	0.379
1989/10/27	-2.7	0.004	0.116
" "	22.0	0.085	0.093
1989/10/28	22.1	0.083	0.101
1989/11/28	21.6	0.086	0.090
" "	45.1	0.008	0.160
1989/11/29	21.8	0.077	0.087
" "	44.1	0.006	0.170
1989/11/30	21.8	0.078	0.087
" "	42.3	0.009	0.120
1989/12/01	21.5	0.075	0.082
" "	43.0	0.013	0.120
1989/12/08	21.1	0.084	0.110
1989/12/18	22.1	0.086	0.099
" "	47.5	0.025	0.190
1990/08/26	21.8	0.089	0.097
" "	37.3	0.014	0.100
" "	48.5	0.008	0.021
1990/08/28	22.3	0.087	0.094
" "	44.0	0.013	0.370
1990/09/11	21.3	0.092	0.096
" "	33.9	0.015	0.095
" "	41.0	0.018	0.076
1990/09/12	21.2	0.089	0.097
" "	37.0	0.073	0.220
" "	55.1	0.015	0.150
1990/09/14	21.5	0.092	0.094
" "	39.5	0.023	0.110
" "	50.6	0.014	0.120
1990/12/09	20.5	0.083	0.084
1990/12/10	20.7	0.079	0.079
" "	33.5	0.014	0.079
1990/12/11	20.6	0.083	0.084
1990/12/12	20.6	0.082	0.084
" "	49.6	0.006	0.200
1990/12/13	20.7	0.083	0.085
" "	31.1	0.004	0.075
1990/12/14	20.9	0.082	0.085
" "	33.5	0.005	0.120
1990/12/15	20.9	0.080	0.080
" "	31.9	0.001	0.059
1990/12/16	20.8	0.084	0.084
" "	43.2	0.003	0.140
1990/12/17	20.8	0.086	0.086
" "	30.6	0.006	0.076

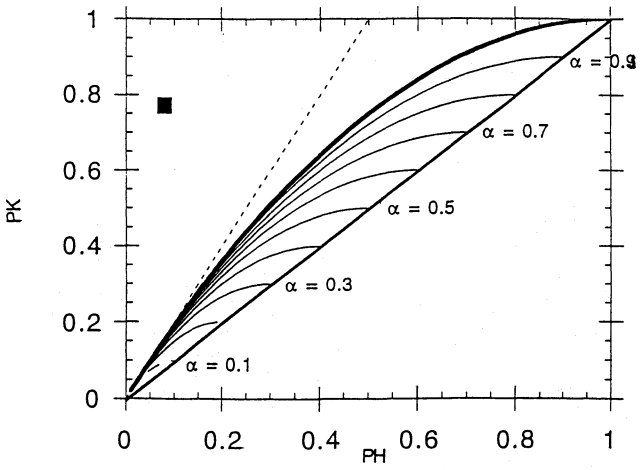

Fig. 5. (p_H, p_K) curves for different values of α, the filling factor of the absorbing cloud. The error box on the measures of p_H and p_K is also given

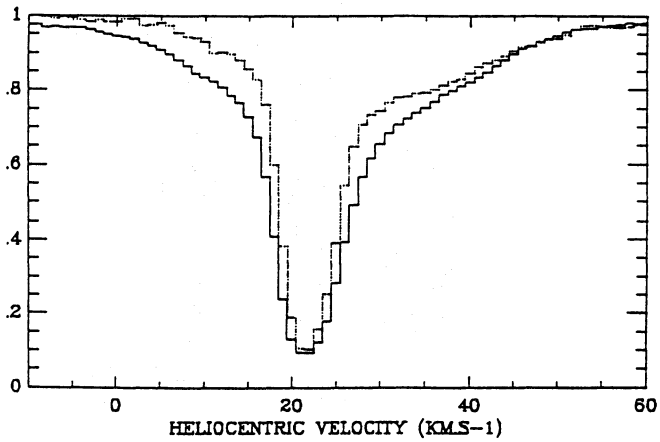

Fig. 6. Superposition of the CS Ca II K (bold) and H (dashed) lines of β Pictoris of Oct. 20, 1989, once reduced in velocity scale. Saturation effects are more important in the red than in the blue. In ordinates, arbitrary units

see that for the blue part ($\simeq -10\ km\,s^{-1}$), α is undetermined, whereas for the red part ($\simeq +20\ km\,s^{-1}$), α is well determined, with a value of about 0.25($\pm$0.20). Similar conclusions are obtained when comparing those H and K spectra divided by reference ones. We can then definitely conclude that at least some part of the infalling gaseous cloud is clumpy with respect to the star.

- variable lines at small redshift ($\leq 60\ km\,s^{-1}$): these lines are the most often observed. For the first time, we are able to see them appearing, on a time scale of a day (Nov. 30/Dec. 1, 1989, Dec. 18/19, 1989, Dec. 09/10, 1990), and disappearing, on a similar time scale (Dec. 18/20, 1989). Noticeably, those lines do not significantly vary on short time scales; i.e. they are stable on time scales of at least 6 hours. In several cases, we even see such components present at the same velocity during several consecutive nights (Dec. 1989, Aug. 1990, Sept. 1990). In the Aug. 1990 sequence, we however note a strong decrease in strength of the variable features between Aug. 25 and Aug. 28. The equivalent width of these lines changes from one observing date to the other, and may be as high as 90 mÅ. In some cases, the features are clearly blended (Aug. and Sept. 1990). Their FWHM is about 0.2 Å. The strength of these components is variable, but the ratio $W_\lambda/FWHM$ is always larger than 0.1 (mean value : 0.15).

In most cases, the lines are not strong enough to yield a measurement of the filling factor. Only in the spectra of Aug. and Sept. 1990, where the variable lines are strong, the size of the cloud can be tested. Unfortunately, for the strongest variable line, obtained on Aug. 25, we have no corresponding Ca II H spectrum. For the remaining spectra of Aug. 1990, α is undetermined, but larger than 0.30. In the spectrum of Sept. 12, we get a value of α ranging between 0.30 and 0.50 for the 13 $km\,s^{-1}$ component, and $\alpha \geq 0.60$ for the 19 $km\,s^{-1}$ component. When comparing both components (see Fig. 7), a saturation effect is clearly present: indeed, both components have the same depth in the H line, whereas they do not in the K line, the 19 $km\,s^{-1}$ component being much deeper. This naturally means that the 13 $km\,s^{-1}$ component is more saturated than the 19 $km\,s^{-1}$ one.

Finally, in the case of Sept. 14, 1990, α is undetermined, but larger than 0.30 for the 13 $km\,s^{-1}$ component, and larger than 0.60 for the 19 $km\,s^{-1}$ one.

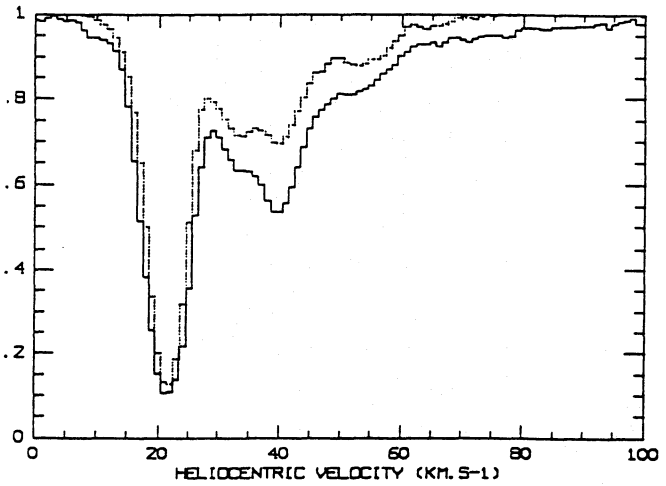

Fig. 7. Same as in Fig. 6, but for the H and K lines of Sept. 12, 1990

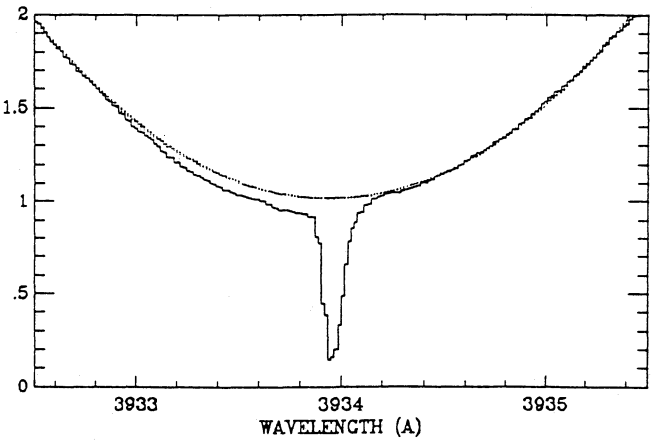

Fig. 8. Superposition of the observed spectrum (bold lines) and the photospheric fit (dashed lines) of Nov. 28, 1989. In ordinates, arbitrary units

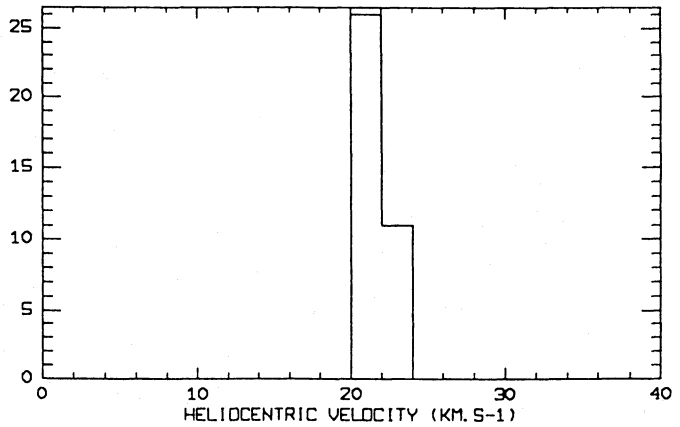

Fig. 9. Histogram of the velocity of the central component. It clearly peaks at 22 km s^{-1}

- variable components at high redshifts (between 54 and 79 km s^{-1}) are also observed (see Fig. 1 and Fig. 2, the spectra recorded on Dec. 01, 1989; Dec. 10, 1990; Dec. 16, 1990), but with characteristics different from the previous ones: most importantly, they vary on short time scales (hours): when present (see Fig. 2), they rapidly spread in velocity; they are broader ($FWHM \geq 0.3$ Å) than those at small redshifts. Because they are larger and are located at the edge of the strong photospheric line, they are not so obvious as those at small redshift, but are however clearly present. For these lines, a precise determination of α is not possible, because the variable features are not deep enough.
- broad and redshifted features: even broader, redshifted features are present, and detected only when dividing the spectra obtained in Dec. 1990 (Fig. 3a). Those broad variable features are not obvious in the non-divided spectra. They are less deep than the previous variable components. Obviously, they cannot be fitted by gaussians, and their shapes indicate peculiar velocity structures. The terminal velocity of the most spectacular one (Dec. 11, 1990) is 160 km s^{-1} with respect to the star, and their equivalent width can be as high as 100 mÅ. They also vary on short time scales (Fig. 3b, Dec. 11, 1990). One remarkable fact is also that they are very similar to those observed in IUE spectra (see Paper VI). Noticeably, this is the first time that so highly redshifted features are detected in the Ca II lines. Also in this case, α cannot be determined.
- for the first time, we clearly detect one blueshifted feature at - 25 km s^{-1} with respect to the star, but only once, in the spectra of Oct. 27, 1989. This blueshifted feature is faint (11 mÅ), but real since confirmed in the Ca II H line (see Fig. 1). α is once again undetermined, due to the weakness of this line.
- also for the first time, we clearly detect a broad blueshifted feature in the spectrum of Nov. 28, 1989, with a terminal velocity of −200 km s^{-1}. This is particularly obvious in Fig. 8, where we show the superposition of the spectrum and of the photospheric fit.

One must note that broad ($FWHM \geq 0.3$Å) and faint ($W_\lambda/FWHM \leq 0.05$) variable features are observed after division by the parabolic fit; these faint features will not be further discussed in the present paper.

3.2. Occurrence of the lines; search for characteristic time scales

3.2.1. The central component

In Fig. 9, we show the histogram of the heliocentric velocity of the central component; it clearly peaks near 22 km s^{-1}. The actual mean value for all available data is 21.5 km s^{-1}. The mean value derived from the data acquired in Dec. 1990 is actually a bit lower, 21 km s^{-1}. However, the difference is at the limit of the precision (see Sect. 2), and it may not be real. Higher precision data would be necessary to see whether the central component is variable on such small velocity ranges (≤ 1 km s^{-1}).

The Fourier analysis of all the velocity positions before 1990 indicates perfect agreement with purely random errors around a constant value.

The histogram of the equivalent widths of this central component (Fig. 10) is relatively broad, spreading between 80 and 110 mÅ (the very small value, 60 mÅ, from Oct. 1989, is due to the strong blend between the central component and the strong variable one, and is not relevant). The spread in equivalent widths is most probably due to artefacts due to the use of different detectors. For instance, it is clear that the equivalent widths measured with the Reticon are systematically smaller than those measured with the CCD (18% is the value estimated from our data). Other

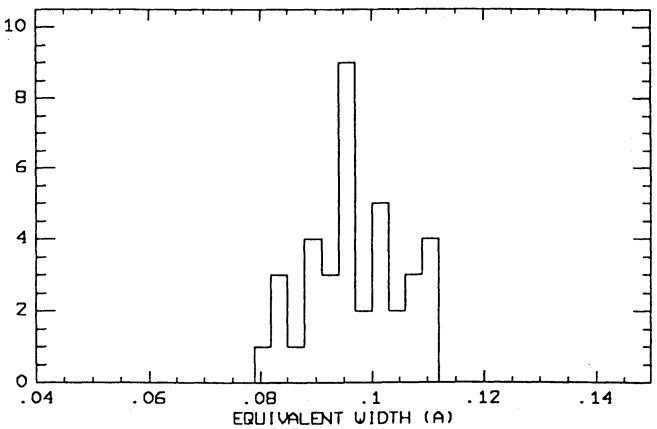

Fig. 10. Histogram of the equivalent width of the central component. The broadness of the histogram is due to the two different detectors (CCD and Reticon)

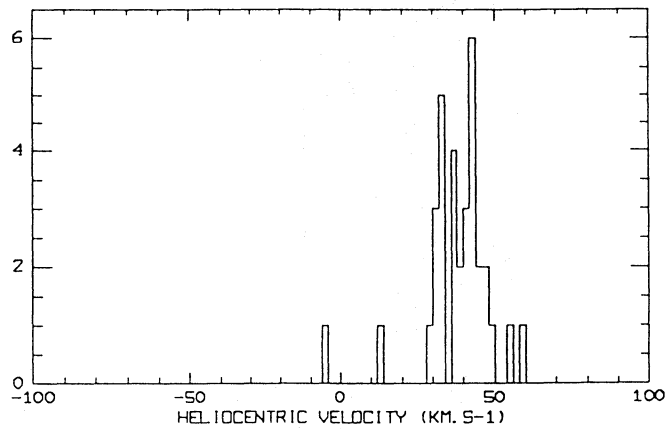

Fig. 12. Histogram of the velocity of the narrow ($FWHM \leq 0.3$ Å and $W_\lambda/FWHM \geq 0.5$) Ca II K variable components observed during this survey

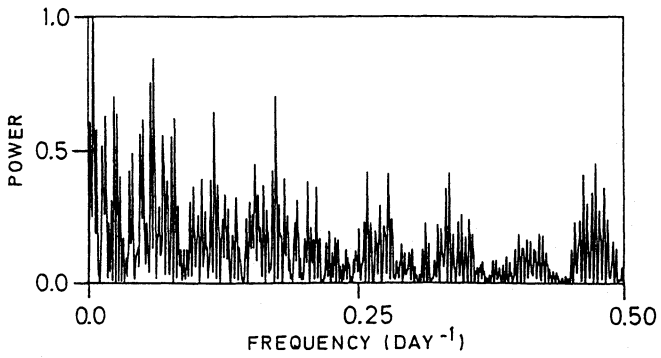

Fig. 11. Power spectrum (Deeming's 1975 method) of the time series of the corrected equivalent widths corresponding to the central component. The absciss gives the frequency in day^{-1}, the ordinate gives the power in arbitrary units

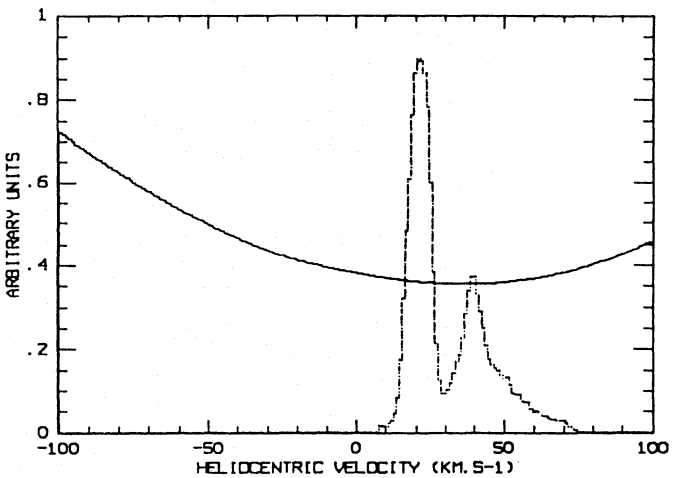

Fig. 13. Superposition of the radiation pressure acting on the Ca II ions as a function of the wavelength (bold lines) and of the CS line (dashed lines) observed on Oct. 14, 1990 (for clarity, the CS lines have been plotted up side down). In ordinates, arbitrary units. A minimum is present at $\simeq$ 20 km s^{-1} with respect to the star in the radiation pressure; the velocity of this minimum is the same as the one of the strongest redshifted variable component

effects such as imperfect subtraction of the dark current, or diffuse light, whose effects are even stronger when the lines are very deep, can explain the remaining discrepancies. The mean equivalent width of the line is 96 m$\AA$, which is in agreement with the values given in previous papers.

Figure 11 shows the power spectrum of the time series of the equivalent widths of the central component once corrected for the above-mentioned instrumental discrepancies (i.e. the equivalent widths measured with the Reticon are corrected by the 18 per cent difference with respect to the ones measured with the CCD). The highest peak is located at low frequencies around 0.005 d^{-1}; it is not significant and corresponds to the fact that the equivalent widths of Aug./Sept. 1990 tend to be somewhat larger. The local deviation from the mean is no more than two standard deviations ($\sigma \simeq 7m\AA$)where σ is the observed dispersion of the data; this value for σ is in good agreement with the expected one. No other peak is outstanding, and the remaining power spectrum is quite indicative of a white-noise process. No periodicity is detected. No characteristic time scale can be outlined. As the dispersion of the measurements can be explained by observational errors, we conclude that the central component does not show evidence for variability in the present data. The latter conclusion also applies to the time series of FWHM.

In summary, the central component does not show definite evidence for variability in velocity, equivalent width or FWHM in the present data.

3.2.2. Narrow variable components ($FWHM \leq 0.3$ Å and $W_\lambda/FWHM \geq 0.5$)

Figure 12 shows the histogram of the velocity of the narrow variable components. It clearly peaks at $\simeq$ 20 km s^{-1} with respect to the star. The actual mean value of this redshift is 40.1 km s^{-1}, heliocentric velocity, and then 18.6 km s^{-1} with respect to the star. This is a very important result and will be discussed in section 4.

A Fourier analysis of the time series of the velocity positions of all the features at about 40 km s^{-1} indicates good agreement with random fluctuations (essentially errors) around a constant value. This outlines the stability in velocity of this component that is present in most of the observing dates.

Power spectra of the equivalent widths have been computed for two corrected time series. For the first one, we applied the same correction as for the central component, i.e. we applied the 18 per cent correcting factor to the Reticon data; for the second one, we assumed the central component equivalent width to be perfectly constant and scaled the narrow component equivalent widths accordingly. The two resulting spectra are quite similar and exhibit an excess of power below frequencies of 0.09 d^{-1}. No significant periodicity is detected. The excess of power indicates that the component could appear to be present during typical time scales of the order of 5-10 days.

3.2.3. Broad components

As already pointed out, we have here no statistical result on these broad lines. All we can give is some numerical information on the individual detected cases. The terminal velocity of the redshifted one observed in Dec. 11, 1989 is $\simeq$ 160 km s^{-1}. The one of the blueshifted feature detected in Nov. 28, 1989 is $\simeq$ -200 km s^{-1}.

4. Discussion

The observations presented here have enabled us to detect a wealth of variable components of new types, and hence to further test our EIB scenario.

4.1. Velocities of the variable lines and time scale variations

4.1.1. Blueshifted features

Two blueshifted features are observed: the narrow one detected on Oct. 27, 1989 (Fig. 1), and the broad one of Nov. 28, 1990, reaching -200 km s^{-1} (Fig. 8). One must note that all these features are much fewer and fainter than those usually observed in the red. Indeed, the broad one only appears when superimposing the spectrum and the photospheric fit.

According to the conclusions of Papers X and XI, one should expect the narrow one with a small blueshift to be reproduced with a larger inclination angle between the axis of the orbit and the line of sight ($\sim 180°$). However, the difficulty here is that the component is very faint. Making the simulations run in the same conditions as those described in Paper X, when changing only the inclination angle, generates a deep component. An explanation can be that the corresponding infalling body produces either a much smaller, or a larger but very thin cloud. However, since in that case no significant measurement for α can be made, it is impossible to distinguish between both cases.

The broad feature of Nov. 28, 1989 (Fig. 8), is easier to interpret. Once the radiation pressure is able to act on them, the Ca II ions begin to move away from the star, and thus spread towards blueshift velocities. Such a broad feature may correspond to the absorption effect of the tail of the ionic cloud of an infalling body, while deeper and sharper components are generated by the head. Indeed, similar features had already been simulated in our previous work. The simulation described in Paper X (Figs. 5–9) shows a deep component with a small redshift, together with many "noisy" features on the blue wing of the line. These blueshifted features are clearly due to the ionic tail, and can be compared to our observed one. The lack of "head" component in this observation may not be surprising. Due to its curvature, the ionic tail might be crossing the line of sight while the head has already moved away.

4.1.2. Centered variable features

We have already shown in Paper XI that those features could be explained by our simulations with a set of orbital values (i.e. the angle between the axis of the orbit and the line of sight, and the perihelion) $(\Phi, q) = (-170, 23)$. This means a somewhat different inclination from Paper X's simulation (the constraint on perihelion is much weaker). This result also appeared to be consistent with the temporal evolution of the lines deduced from the model of Paper XII.

The size of the cloud we can estimate is about 40% of the stellar surface, which is in good agreement with the results of the simulations.

4.1.3. Highly redshifted features

The observed velocities of some of the variable components are much higher than what we usually detect in the Ca II K lines, and are more comparable to those observed in the UV lines. Moreover, the components present somewhat different characteristics than those at small redshifts, in particular, shorter time scale variability.

We have shown in Paper XI that we could explain such highly redshifted components, when considering a closer approach of the infalling body ($\simeq 5R_*$), compared to what we need to explain the variable features at 20 km s^{-1} (typically 20 R_*), without changing any other parameter. In that case, the simulation predicts highly redshifted features, much broader than the components at 20 km s^{-1}, in total agreement with the observations. The simulations also predict an absorbing cloud significantly smaller than the stellar surface (the radiation pressure being indeed much higher close to the star). Unfortunately, this last point cannot be tested with the present data, since we cannot make any significant measurement for α. Note that nevertheless, the data are certainly not in contradiction with this fact.

These highly redshifted features evolve on time scales shorter than those at lower redshifts. This is again not surprising: when closer to the star, the orbital velocity of the body is higher and it crosses the line of sight more rapidly. Indeed, the higher the redshift of a variable feature, the smaller its variation time scale is expected to be (this intended for bodies with similar inclinations). This output of the simulations (Paper X), is then in good agreement with the observations.

The detection in the divided spectra of highly redshifted (+160 km s^{-1}) and very broad features on Dec. 11 and 16, 1990 confirms the conclusions of Papers X and XI. These features, which behave like those of the UV lines, are simply produced by bodies having an even closer approach, i.e. very few stellar radii, which corresponds then to typical approaches of bodies producing highly redshifted UV features (Paper X). Due to the very high radiation pressure, such bodies have very small Ca II clouds, leading to almost unobservable absorption features. This is not the case for other ions (Mg II, Al III) for which the radiation pressure is much smaller. Highly redshifted (one could say "UV-like") Ca II absorption features are thus expected to exist, although much fainter.

4.1.4. Narrow variable components at small redshift

A major output of this survey is that we often observe variable components at about 20 km s^{-1} with respect to the star. This also corresponds to the velocity of the variable line observed in

1985–86 (Paper V). Furthermore, these lines are stable on time scales of at least 6 hours.

In Paper X, we have shown that the EIB scenario could explain these lines, with $(\Phi, q) = (-150, 23)$, the constraint being much stronger on the angle between the axis of the orbit and the line of sight than on the perihelion.

However, the simulation predicts that the variable lines due to one event are present during a time scale (~4 hours) shorter than the one we observe. We proposed in paper X that a long lasting event could be in fact due to several individual objects crossing the line of sight roughly at the same moment, but with spread out perihelions. This could also explain the multistructures we had in some variable lines. These several bodies do not have to fall on the same orbit, in a simple queue. The only constraint is on the inclination of the orbit. Indeed, bodies crossing the line of sight at different stellar distances, larger than 10–15 R_*, and having the same orbital inclination with respect to the line of sight, should produce very similar absorption features. In such a case, the present data imply that the rate of infalling bodies is high enough to allow the variable components to be observed longer than in the case of one single event. This may be also consistent with the very high observing frequency of such variable features, and with the observations of multiple events.

We also tried to find additional physical effects which could tend to stabilize the components once produced, so as to observe them on longer time scales. One possible way is to take into account the velocity dependence of the forces which act on the ions. In the past simulations (see paper IX, X and XI), we took into account the gravity, radiation pressure and collisions. All these forces were assumed to be constant, independent of the velocity. In particular, the radiation pressure was calculated using the flux at the bottom of the Ca II K and Ca II H lines. Indeed, the real radiation pressure is more complex and actually depends on the stellar flux, i.e. on the shape of the Ca II K and Ca II H lines. It also depends on the H_ϵ stellar line, which is blended with Ca II H one. The resulting shape is shown in Fig. 13, where the dependence on the wavelength is clear. This might have important effects on the motion of the ions. Indeed, if we assume that the ions are produced at a constant rate (which seems to be a reasonnable assumption, see paper X) $dn/dt = \text{cst}$, and are submitted to the forces $\sum F(v)$, the equation of motion of the ions is given by

$$\frac{m dv}{dt} = \sum F(v). \tag{5}$$

We get then

$$\frac{dn}{dv} = \frac{dn/dt}{dv/dt} = \frac{m.dn/dt}{\sum F(v)} = \frac{\text{cst}}{\sum F(v)}. \tag{6}$$

We see then that dn/dv will reach a maximum value for the minimum value of $\sum F(v)$. Taking into account the dependence of the radiation pressure as a function of v, we see that dn/dv will reach a maximum when the radiation pressure will be minimum. Thus, there will be an accumulation of ions at the minimum of the radiation pressure. Figure 13 shows that this minimum occurs at about 20 km s^{-1} with respect to the star. Moreover, this effect can be cumulative, because the more ions at this velocity, the more important the minimum of the radiation pressure will most probably be. This very simple calculation predicts an accumulation of ions at this velocity and may provide an explanation to the stability of the components at 20 km s^{-1}. However, it is quantitatively not clear whether this effect is strong enough is to efficiently stabilize the components. New simulations are underway to quantitatively test this effect and will be presented in a forthcoming paper.

4.2. Occurrence of variable events

4.2.1. Global rate of variable events

From this survey, we can derive a rate of variable events. If we suppose that each variable line observed during one night is due to the same event, then we derive a rate of 24 events for 38 observing dates, which means 230 per year. This is an approximate value, because if the long lasting events are due to several bodies, the actual rate will be higher, and on the contrary, if the events last more than one night, the actual rate will be lower.

This high rate of events is a bit less than the one derived from IUE data. However, the signatures of infalls are much more pronounced in the UV lines of Al III or Mg II, from which the rate was derived, than in the Ca II ones. This difference of behaviour has already been discussed and simulated in Paper X and shown to be related to the fact that the UV lines are seen in the case of closer approach than the Ca II ones.

4.2.2. Rate of observation of the different lines and time evolution

We have seen that we observed more events at 20 km s^{-1} with respect to the star than at other velocities. In Paper X, we have suggested that the velocity of the components is directly linked with the inclination of the orbital axis of the infalling body, and that the presence of a perturbing body could explain the variation of these velocities as a function of time. In particular, we showed that the component at 20 km s^{-1} had to be due to bodies arriving with an inclination of $-150 \pm 10°$.

In Paper XII, a model had been developed involving planetary perturbations by a planet on an elliptical orbit around the star. The best fit with the observational data available at that time gave a planet with an eccentricity $\simeq 0.65$, semi-major axis $\simeq 3.2$ A U, and angle between the major axis of the orbit and the line of sight $\simeq 80°$. According to this fit, the rate of variable events should vary drastically over the orbital period of the planet. Furthermore, it showed that most of the events that may occur in Ca II (only the sharp and deep ones are involved) should have redshifts remaining between 0 and 50 km s^{-1}. This is still consistent with our data.

More precisely, this study predicted a sudden peak of event frequency at redshift $\simeq 0$ km s^{-1} after a long period without any activity. These events should remain numerous and move towards redshift $\simeq 20$ km s^{-1} within two months. We have tentatively identified this peak to the observed scenario of late 1989, also displayed in the present paper (Fig. 1).

The scenario predicts a subsequent long decrease of the events frequency, making it ~ 6 times less one year after the peak, while the redshift of the Ca II events remains in the same range. It also predicted the appearance of UV events within this year with growing redshifts, up to 200 km s^{-1} (even higher velocity events coming afterwards).

According to Paper XII, the set of data presented here should correspond to that particular year. It is clearly impossible to confirm or infirm definitely Paper XII's scenario. However, some facts can be noted :

1. The redshifts of the main Ca II events (i.e. the sharp and deep ones) remain in the predicted range, the peak of the histogram at 20 km s^{-1} being even a bit puzzling.
2. The very faint and broad features at $\simeq$ 160 km s^{-1} detected in December 1990 have been identified as the signature in Ca II lines of bodies able to produce UV events, i.e. bodies with very close approaches to the star (very few stellar radii). This may indicate that UV events with such redshifts have been generated, particularly at the end of the surveyed year, which is in agreement with the predictions.
3. Deriving an evolution of the event frequency from our data is difficult, just because we don't have daily observations all over the year. It is however tempting to compare the set of data gathered in December 1989 to the one of December 1990 (Fig. 1). The comparison is justified because the data are numerous in both cases: the activity in december 1990 seems to be somewhat less than one year earlier, which would be consistent with the model, although a variation by a factor 6 is not observed. This could however be easily explained by density variations of kilometer size bodies within the disk.

4.3. Mass of the absorbing cloud

If we calculate the total abundance of Ca in the same way as we did in paper VI, i.e. supposing that all the Ca is singly ionized, we get for a typical 100 m$\mathring{A}$ equivalent width variable component, a total of about 2. 10^{35} Ca atoms in the cloud. When scaling to the solar or meteoritic abundances (as we also did in paper VI), we find a total mass for the body comparable to the one derived from UV data, within a factor $\simeq$ 2, which leads to a typical 1 km size for the solid body (assuming a density equal to unity). The remarks given in paper VI also apply to the present calculation.

4.4. Size of the absorbing cloud

The present observations have shown that in some cases, the absorbing cloud was clumpy with respect to the stellar surface. This is in excellent agreement with our simulations which predict that the Ca II cloud has a size smaller than the stellar surface; it strongly ascertains our EIB scenario.

5. Summary of the results and conclusion

Numerous variable lines have been detected at different velocities during the present 15 month survey. In particular, variable features never observed up to now, have been detected at high redshifts and also in the blue. An important output of this survey is that blueshifted features are very much less frequent than redshifted ones, which seems to be in agreement with the simulations developed in Paper XII. The most redshifted components vary much more rapidly than the less redshifted ones. All this is consistent with our EIB scenario.

The present observations also confirm the predictions of the EIB scenario concerning the size of the Ca II absorbing cloud, which is shown to be smaller than the stellar surface ($\simeq$ 40 per cent). Indeed, the major output of this study is that we definitely proved the clumpy structure of the infalling gas. The rate of infall derived here, about 200 per year, is comparable to the one derived in Paper VII, and compatible with the predictions of paper XII. The mass of infalling bodies is also comparable.

The global evolution of the lines over the year 1990 seems to be in agreement with the formerly predicted scenario involving perturbations by a planet on an elliptical orbit in the disk. However, it is still impossible to definitely confirm or infirm such an hypothesis, essentially because the evolution of the rate of infall as a function of time is poorly known. Obviously, continuous observations over very long periods are needed to study the rate of infall as a function of time, and then to test the possible presence of a perturbing body.

Another important result is the fact that when variable features are observed, their velocity is most of the time at 20 km s^{-1} with respect to the star. This observational fact can be explained by the presence of several bodies falling to the star with a same inclination angle, not necessarily the same perihelions, or/and by additional physical effects, such as the dependence of the radiation pressure as a function of the velocity. New simulations of both scenari will be presented in a forthcoming paper.

Acknowledgements. We are indebted to J. Melnick from ESO La Silla, who enabled us to get spectra of β Pictoris via different observers, namely Drs Vladilo, Centurion, Jankov, Pallaviccini, Waelkens and Zhao. We kindly thank these observers. We also thank M. Saffon who greatly contributed to this work, A. Smette who helped managing with some MIDAS procedures, and D. Baade for fruitful discussions. We also would like to thank the referee, Dr Bruhweiler, for his carefull reading of the paper and his fruitfull comments. Finally, we also thank C. Ounnas and G. Dobbels for their kind help during remote control observations.

References

Beust, H., Lagrange-Henri, A.M., Vidal-Madjar, A., Ferlet, R., 1989, A&A 223, 304 (Paper IX)
Beust, H., Lagrange-Henri, A.M., Vidal-Madjar, A., Ferlet, R., 1990, A&A 236, 202 (Paper X)
Beust, H., Vidal-Madjar, A., Ferlet, R., Lagrange-Henri, A.M., 1991a, A&A 241, 488 (Paper XI)
Beust, H., Vidal-Madjar, A., Ferlet, R., 1991b, A&A 247, 505 (Paper XII)
Bruhweiler, F.C., Kondo, Y., Grady, C.A., 1991, ApJ 371, L27
Deeming, T.J., 1975, Ap&SS 36, 137
Ferlet, R., Hobbs, L.M., Vidal-Madjar, A., 1987, A&A 185, 267 (Paper V)
Grady , C.A, Bruhweiler, F.C., Cheng, K.-P., Chiu, W.A., Kondo, Y., 1991, ApJ 367, 296
Lagrange, A.M, Ferlet, R., Vidal-Madjar, A., 1987, A&A 173, 289 (Paper IV)
Lagrange-Henri, A.M., Beust, H., Vidal-Madjar, A., Ferlet, R., 1989, A&A 215, L5 (Paper VIII)
Lagrange-Henri, A.M., Vidal-Madjar, A., Ferlet, R., 1988, A&A 190, 275 (Paper VI)
Norman C.A., Paresce, F., 1989, The formation and evolution of protoplanetary systems, ed. Weaver and Danley, Cambridge Univ. Press
Scargle, J.D., 1972, ApJ 263, 835

This article was processed by the author using Springer-Verlag LaTeX A&A style file 1990.